Design of the optical system for the gamma factory proof of principle experiment at the CERN Super Proton Synchrotron

Aurélien Martens,* Kevin Cassou, Ronic Chiche, Kevin Dupraz, Daniele Nutarelli, Yann Peinaud, and Fabian Zomer
Université Paris-Saclay, CNRS/IN2P3, IJCLab, 91405 Orsay, France

Yann Dutheil, Brennan Goddard, Mieczyslaw Witold Krasny, Thibaut Lefevre, and Francesco Maria Velotti
CERN, CH-1211, Geneva, Switzerland

(Received 22 April 2022; accepted 26 September 2022; published 7 October 2022)

The Gamma Factory proof of principle experiment aims at colliding laser pulses with ultrarelativistic partially stripped ion beams at the CERN Super Proton Synchrotron. Its goals include the first demonstration of fast cooling of *ultrarelativistic* ion beams and opening up many possibilities for new physics measurements in various domains from atomic physics to particle physics. A high average-power, pulsed laser system delivering approximately 200 kW needs to be implemented for this aim. This is possible thanks to state-of-the-art optical systems that recently demonstrated similar performances in the laboratory environment. Challenges lie in the implementation of this kind of laser system in the harsh environment of hadronic machines including their robust and fully remote operation. The design of this laser system, involving a high quality factor enhancement cavity, is drawn and described in this article. Mitigation procedures are proposed to overcome limitations imposed by the occurrence of degenerate high-order mode at high average power in such optical resonators. We show that the operation at average power above 200 kW is feasible.

DOI: 10.1103/PhysRevAccelBeams.25.101601

I. INTRODUCTION

The Gamma Factory (GF) is an innovative concept [1] aiming at producing unprecedented rates of photons, up to 10^{18} per second, of energies ranging up to 400 MeV thanks to the interaction of a laser beam with ultrarelativistic partially stripped ion beams. This concept could be implemented in existing hadronic storage rings. It could thus greatly extend the physics scope of such accelerators. The physics scope addressed by this concept covers atomic physics [2,3], applied [4], and fundamental [5,6] nuclear physics, particle physics [7–9] including new physics searches [10,11], and accelerator physics [7]. The laser beam can be optimized to achieve fast, within a few seconds, cooling of high energy hadronic beams which are beyond the reach of the present cooling methods of such beams [7]. The GF concept introduces as well new techniques to produce high rates of high quality beams of positrons, pions, muons, and neutrinos [12].

In order to demonstrate that this scheme is technically feasible, a proof of principle experiment (POP) is planned at the CERN Super Proton Synchrotron (SPS) [13]. The main goal is to install and operate in the demanding environment of hadronic storage rings an optical system representative of that which would be ultimately implemented in the Large Hadron Collider (LHC). Several physics results are also expected as the outcome of this experiment. They include atomic physics measurements with highly charged ions and—more importantly for the future of this concept—the demonstration of fast cooling of ultrarelativistic ion beams [7].

For the POP experiment, the requirements of single laser pulse energy and average power imply, as shown in Sec. III, the installation of an optical resonator in an SPS tunnel. A similar configuration, where a Fabry-Perot cavity (FPC) was integrated and operated in an electron ring accelerator, had been realized in the past [14–17] for various inverse Compton scattering applications. Recent designs of such systems are assuming relatively small electron beam sizes of few tens of micrometers at the interaction point (IP) of laser and electron beams and a similarly small laser spot size. This application generally requires independent

*aurelien.martens@ijclab.in2p3.fr

tuning of the laser spot size and the cavity length, which has to correspond to the period of arrival of electrons at the IP. To this end, four-mirror bow-tie geometries are employed [18]. Such a solution will likely be followed for the implementation of the optical resonators in the LHC rings. However, the design of the Gamma Factory POP experiment must account for the specificity of the interaction with the hadronic beams of the SPS and the corresponding major integration constraints. In particular, peculiar attention was paid to avoid the modification of the present SPS ring optics, which implies to refrain from designing and implementing an optimal POP experiment IP optics. As a consequence and given the restricted places where Fabry-Perot resonator can be implemented, the hadronic beam transverse size at the photon-ion collision IP is large, of millimeter scale, and the radiation environment is significantly harsher than that of the low energy and low average current electron rings.

The design of the optical system required to reach the goals of the POP is described in this paper. It is organized as follows: In Sec. II, the expected ion beam parameters and location of the POP experiment in the CERN SPS are described. In Sec. III, the optical system considered for the experiment is specified. A summary of the expected performance is provided in the Conclusion.

II. THE PROOF OF PRINCIPLE EXPERIMENT

In this section, the general layout of the proof of principle experiment, as well as the hadronic beam parameters, is described.

A. Ion beam

The ion beam species for the POP experiment has been chosen [13] such that (i) the ion beam lifetime, mainly limited by the residual pressure of approximately 1.2×10^{-8} mbar could be long enough in the SPS, typically several tens of seconds, to allow the demonstration of beam cooling, (ii) an atomic resonance lies within an energy range that can be accessed with a feasible laser system and its excited state lifetime is short enough so that a *beam* of photons is thus produced and measured with a simple detection system as scintillating crystal coupled to a camera, and (iii) it can be produced with the existing injectors of the CERN accelerator complex.

A unique species, $^{208}Pb^{79+}$ sometimes dubbed lithiumlike lead in the literature, has been found to fulfill all of these requirements since its $2s \rightarrow 2p_{1/2}$ transition occurs at 230.81 eV and the lifetime of the excited state is of 76.6 ps, according to calculations [19]. It must be noted that there is no measurement of this quantity for this species, while similar calculations are consistent with experiments for lithiumlike xenon with experimental accuracy of less than one per mille [20–25]. The expected beam lifetime of approximately 100 s in the SPS for $^{208}Pb^{79+}$ has been extrapolated from measurements made with $^{208}Pb^{80+}$ and $^{208}Pb^{81+}$ [26]. A movable foil allows stripping $^{208}Pb^{54+}$ into $^{208}Pb^{79+}$ in the injection line of the SPS with an expected efficiency of 35% [27]. Operation of the POP in parallel with other activities requires that the foil can be inserted and removed on a cycle-to-cycle basis. In that case, the maximum allowed duration of the circulation of the ion beam at the maximum energy (flattop) is 10 s. The POP experiment will last over a large number of injections. Two different filling patterns are possible [28]: (i) Four bunches separated by 100 ns and up to nine injections separated by 150 ns and (ii) three bunches separated by 75 ns and up to 12 injections separated by 150 ns.

B. Location of the experiment

It is foreseen to locate the experiment in a straight section of the SPS, aside a decommissioned tunnel which was used to inject the SPS positron beam into the LEP collider. The latter will be used to install an optical room where the laser system will be placed, see Fig. 1. It naturally allows to reduce the radiation dose that may be delivered to the laser system and that is generated by losses of hadrons while beams are circulating all over the year in the SPS ring. Indeed, the lifetime of the laser and its amplifiers would certainly be strongly affected if installed too close to the SPS beamline [29–31]. Strong bumper magnets are also located nearby upstream of this half-cell 621, which allows to steer the beam at its flattop energy and optimizes alignments. Cavity mirrors are not expected to age with the expected integrated dose of 10 Gy per year [29,32,33] at the beam height corresponding to less than 10^{10} high energy particles and thermal neutrons per squared centimeter, as estimated from *in situ* measurements performed in 2018. This integrated dose is largely dominated by the contribution from the proton run and will allow to switch off the supply of a few remaining elements such as cameras, photodiodes, and motors.

The corresponding ion beam parameters are summarized in Table I, where $\alpha_{x,y}$, $\beta_{x,y}$, and $\gamma_{x,y}$ are Twiss parameters, $\eta_{x,y}$ and $\eta'_{x,y}$ are momentum dispersions.

The evolution of the beam size and optical functions around the proposed POP experiment location are shown in Fig. 2. To ensure that the POP does not interfere with nominal SPS operation, a *stay-clear* region around the reference beam axis, which needs to be kept free of any element, is defined. It is computed, in the horizontal plane, based on the maximum excursions of the (i) injected proton fixed target beam at 14 GeV/c and a 12 mm mrad (horizontal) normalized emittance, along with related alignment error and tolerances; (ii) the slowly extracted separatrix with 400 GeV/c protons on the 1/3 resonance (asymmetric); and (iii) the bumped or extracted beam, although not a concern in the region considered. For the

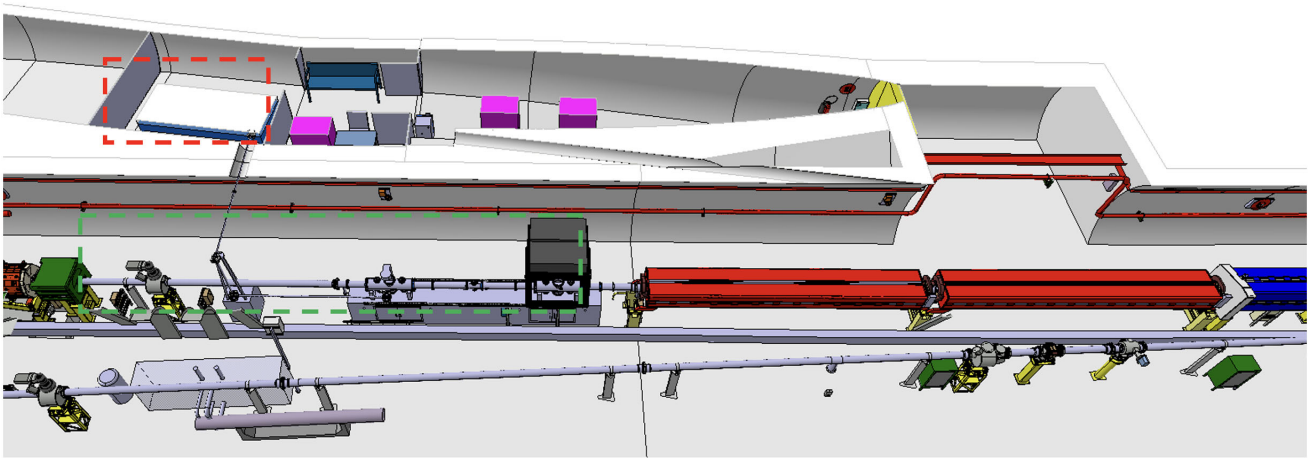

FIG. 1. Model of the location of the Gamma Factory POP experiment in the SPS showing the TI18 tunnel on the top, the SPS ring in the middle, and the TT60 extraction line on the bottom with the partially stripped ion beam traveling from the right to the left. The model shows the foreseen location of the Fabry-Perot cavity in the SPS ring (green dashed box), the location of the optical room (red dashed box), and the laser transport line in between the two.

TABLE I. $^{208}Pb^{79+}$ bunch parameters in the SPS. Ions per bunch at injection are obtained from Ref. [34] for the fully stripped lead ions, scaled by the stripping efficiency of $^{208}Pb^{79+}$ extrapolated from experimental data and calibrated simulations [13,35,36]. The parameters $\alpha_{x,y}$, $\beta x, y$, and $\gamma_{x,y} = (1 + \alpha_{x,y}^2)/\beta_{x,y}$ are the Courant-Snyder parameters, $\eta_{x,y}$ represents the dispersion, and $\eta'_{x,y}$ is the angular dispersion. The beam spatial and angular spreads are denoted $\sigma_{x,y}$ and $\sigma_{x',y'}$, respectively.

Parameter name	Value
Bunch length at flat top	213 ps
σ_E/E—rms relative energy spread	2×10^{-4}
Expected lifetime	100 s
Maximum number of bunches in the ring	36
Revolution frequency f_{rev} ($\gamma = 96$)	43.373 kHz
rf frequency f_{rf}	200.384 MHz
m—ion mass	193.687 GeV/c^2
E—mean ion beam energy	18.652 TeV
Mean Lorentz relativistic factor γ	96.3
N—number ions per bunch at injection	9×10^7
Normalized transverse emittance	1.5 mm mrad
α_x	−1.549
β_x	55.32 m
η_x	2.462 m
η'_x	0.0976
α_y	1.301
β_y	43.87 m
η_y	0.0 m
η'_y	0.0
$\sigma_{x'} = \sqrt{\epsilon_x\gamma_x + (\sigma_E/E\eta'_x)^2}$	3.66×10^{-5}
$\sigma_{y'} = \sqrt{\epsilon_y\gamma_y + (\sigma_E/E\eta'_y)^2}$	3.09×10^{-5}
$\sigma_x = \sqrt{\epsilon_x\beta_x + (\sigma_E/E\eta_x)^2}$	1.05×10^{-3} m
$\sigma_y = \sqrt{\epsilon_y\beta_y + (\sigma_E/E\eta_x)^2}$	8.27×10^{-4} m

vertical plane, only the injected proton fixed target at 14 GeV/c and an 8-mm mrad normalized emittance is considered, with the related alignment error and tolerances. The resulting stay-clear regions in each plane are shown as dotted lines in Fig. 2. The aperture of the SPS magnetic elements is sized to roughly follow the envelope of the largest accelerated beams and we can see that the stay-clear region is very close to the apertures of the elements on either side of the region considered. The *stay-clear* region is numerically 90×45 mm^2 (in horizontal × vertical planes) at the entrance of the optical cavity and 108×38 mm^2 at the exit. At the location considered for the x-ray detector ($s = 6458$ m), the stay-clear region is 118×34 mm^2.

The stability of the closed orbit of the SPS has been estimated from past measurements and from estimated drifts of alignments and aging of beam position monitors that in turn affect the optimization of the closed orbit correction. At the GF POP location, the stability of the beam energy and magnetic field in the SPS also affects the beam position. All these aspects put together, a transverse stability of the ion beam of approximately 0.45 mm (0.30 mm) in the horizontal (vertical) direction is obtained. It is judged enough for the operation of the POP.

The x-ray detector is composed of a scintillating crystal (YAG:Ce) and a camera to image the scintillation light. This type of system has been employed elsewhere in the CERN accelerator complex and proved its robustness [37].

III. DESIGN OF THE OPTICAL SYSTEM

In order to meet the constraints imposed by the ion beam parameters and the physics objectives, as ion beam cooling in a short enough time to observe its effects given the

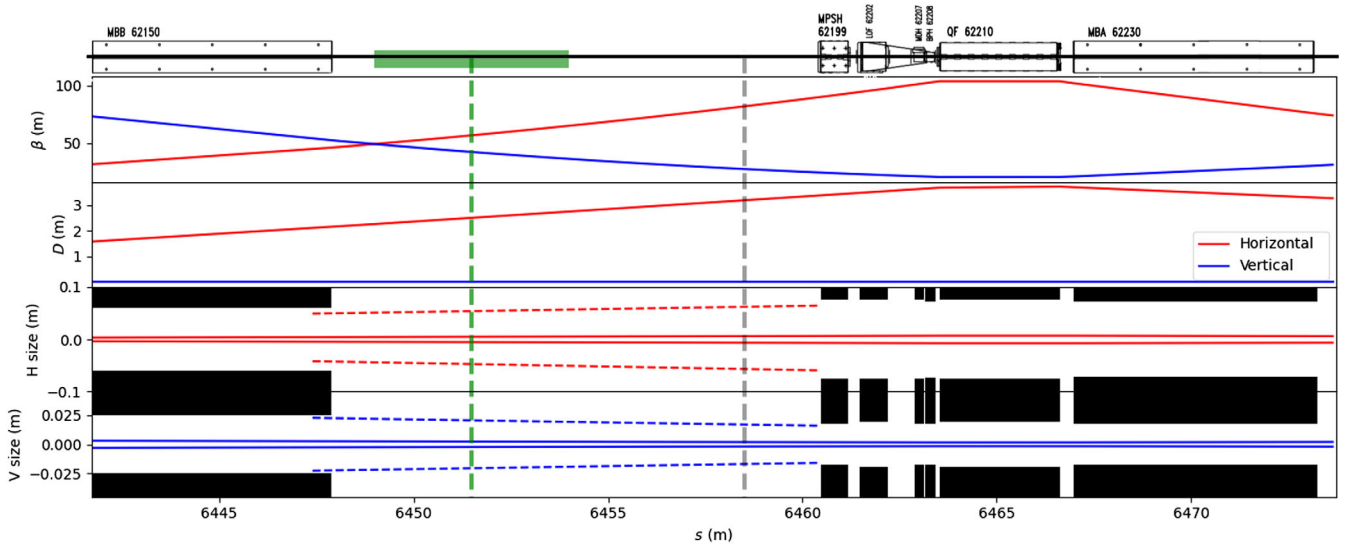

FIG. 2. Layout (top), betatron and dispersion functions (middle), and horizontal and vertical beam sizes as a function of the coordinate of the SPS ring (bottom). The beam goes from left to right. The layout clearly exhibits from left to right, a dipole magnet, in green the location of the Fabry-Perot cavity described in this paper, a corrector, an octupole, a BPM, another quadrupole, and a dipole. The betatron and dispersion functions for the horizontal and vertical directions are shown in red and blue, respectively. Note that there is no vertical dispersion while the horizontal dispersion is about 2 m at the interaction point between ions and the laser, approximately identified with the green dashed line. The vertical gray dashed line represents the location of an x-ray detector that will be installed to measure the scattered photons. The rms beam size is depicted by the plain double red (horizontal) and blue (vertical line) of the bottom plots. Black boxes represent the aperture of the magnetic elements. The dashed red and blue lines represent the *stay-clear* regions described in the text.

limited ion beam lifetime in the ring, it is necessary to construct a laser system delivering pulses of up to 5 mJ with laser pulses rms durations σ_t in the range of several picoseconds [7,38]. Table II summarizes the considered laser parameters, where the rms transverse intensity distribution at IP is denoted σ_T. In order to demonstrate operations schemes similar to those envisioned for the future of Gamma Factory, multibunch operation is sought. Thus a 40-MHz operating frequency of the laser, compatible with all the running modes of the SPS and LHC beams is chosen. Overall, the above two requirements call for a 200 kW laser system that must stably be operated in the SPS. This level of power can be reached by implementing an optical resonator seeded by a mode-lock laser oscillator amplified to several tens of Watts. Such a system has already been realized and demonstrated to be stably operable in the well-controlled environment of an optical room [39] though with a different optical geometry.

TABLE II. Laser parameters for the Gamma Factory POP experiment. The wavelength is given by the choice of the ion species and the availability of high power systems. The single pulse energy U and pulse duration σ_t are determined to maximize the number of excited atoms at each bunch crossing, see Ref. [13] for details. The relative spectral width is obtained from the pulse duration by assuming Fourier limited laser pulses. The crossing angle θ_L and the laser-beam rms transverse size of the intensity distribution σ_T are constrained by the mechanical implementation and the optical design, respectively, see text for details.

Parameter name	Value
λ—wavelength	1034 nm
σ_λ/λ—rms relative spectral width	2×10^{-4}
U—single pulse energy at IP	5 mJ
σ_T	0.65 mm
σ_t	2.8 ps
θ_L—collision angle	2.6°

The laser system consists of three elements, namely the seed laser, a high power laser amplifier, and an optical resonator that is used to passively amplify the laser pulse energy at the interaction point. A similar system has already been operated in accelerator environments for some time, see for instance Ref. [16], though with a reduced average power. The ThomX project [17] is being commissioned with similar optical performances. Operations and maintenance works will however be simplified in the ThomX case due to its reduced radiation field compared to that of the SPS. The major novelty of the design of the Gamma Factory optical system lies in the stringent requirement of its remote operation and the necessary robustness of the system. In addition, a laser transport line needs to be carefully designed to link the laser room and the optical resonator located in the SPS ring. It will have to be operated under vacuum and with dedicated steering and pointing stabilization devices to ensure an excellent coupling to the optical cavity.

Since, in any case, a passive optical cavity needs to be implemented to reach the objectives due to the high average power required, the design of the optical system, as a whole, is driven by reasonable performance compromises. A too large quality factor of this optical cavity would induce too strong constraints on the seed laser phase noise characteristics, as explained below. A too small quality factor would involve a laser average power of several hundreds of Watts [40] which would require the implementation of cryogenic cooling [41], a significantly larger plug power, and a significantly increased cost. This kind of system, which to the best of the knowledge of the authors, is not industrialized, induces increased operational risks that are critical for the POP experiment. The design described below tends to find a compromise between these two extreme cases.

A. Laser oscillator and amplifier

The laser system is composed of a seed laser oscillator and a power amplifier delivering at least 50 W of average power at 40-MHz pulse repetition rate. In order to allow the lock and maintain an efficient coupling [42,43] of the amplified seed laser with the passive optical resonator, the seed laser optical spectrum must be maintained within the filtering lines of the optical cavity [44]. It implies, in particular, that the laser repetition rate and the free spectral range of the cavity are matched. This is possible if the seed laser is a femtosecond, passively mode-lock frequency comb. It requires intracavity piezoelectric actuator and a stable coarse tuning stage, often realized with a motorized translation stage to adjust the repetition rate of this passively mode-lock laser oscillator. Such a slow tuning capability of the repetition rate is also generally needed to slowly follow the low drifts of a reference clock. This reference clock, common to the laser system and the accelerator, ensuring their synchronous operation, will be placed nearby the optical system. This clock is transmitted to the accelerator control so that the ion revolution frequency is locked on it, in a similar manner as done for the AWAKE experiment [45]. The laser must exhibit excellent phase stability in order to be efficiently locked on the long and high-quality factor Fabry-Perot cavity. This requirement turns out to constrain heavily the choice of the laser, despite the use of feedback loops with a few kilo-Hertz bandwidths, and even hundreds of kilo-Hertz in several cases. The rms variation of the frequency δf_{rms}, obtained from integration of the frequency power spectral density (PSD), corrected for feedback and optical cavity filtering, is used as an estimation of the laser linewidth. It can be compared to the Fabry-Perot natural bandwidth $\Delta f = \mathrm{FSR}/2\mathcal{F}$, where FSR is the cavity free spectral range an $\mathcal{F}$ its Finesse. This is justified since the coupling loss to the cavity, related to phase noise in the laser, is approximately

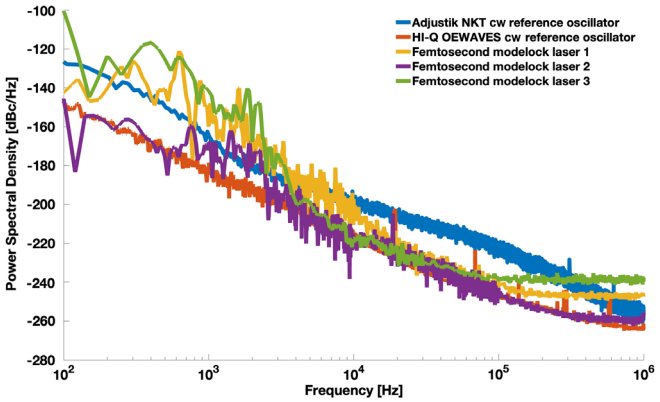

FIG. 3. Top: power spectral density of phase noise measured from self heterodyne beating for two cw reference oscillators and heterodyne beating with the HighQ OEwaves cw reference oscillator for three commercial femtosecond mode-lock oscillators. The phase noise PSD is shown for a carrier frequency of 40 MHz that corresponds to the repetition frequency required for the Gamma Factory POP experiment.

$$\left(\frac{\delta f_{\mathrm{rms}}}{\Delta f}\right)^2,$$

if $\delta f_{\mathrm{rms}} \ll \Delta f$. With a FSR $= 40$ MHz and $\mathcal{F} = 10{,}000$, the corresponding typical acceptable laser oscillator linewidth must be well below 2 kHz. This requirement typically corresponds to a case where the laser noise is well below that of the Adjustik NKT cw reference oscillator for which phase noise single-sided power spectral density $L(f)$ is given in Fig. 3. It is measured by self heterodyne beating. In this figure, the measurements for three different commercial oscillators, representative of those that could be used for the Gamma Factory POP experiment, are also shown. These measurements are made by heterodyne beating against an OEWaves HighQ ultrastable cw reference, for which self-heterodyne beating phase noise is also shown in the figure. The measurement noise floor is visible above 100 kHz on the pulsed laser measurements and depends on the actual average power of the laser itself. We then compute

$$\delta f_{\mathrm{rms}[f_1;f_2]} = \sqrt{\int_{f_1}^{f_2} f^2 L(f) |H_c(f)|^2 |H_{fb}(f)|^2 df}$$

for two different ranges of frequency that are chosen as $[0.1;3]$ kHz and $[3;1000]$ kHz. The $H_c(f)$ denotes the transfer function of the optical cavity and $H_{\mathrm{fb}}(f)$ represents the feedback transfer function. The results are summarized in Table III. We assume that $H_{\mathrm{fb}}(f) = 1/[1 + H(f)]$ with $H(f) = -if_{\mathrm{fb}}/f$, the transfer function of a pure integrator and where $f_{\mathrm{fb}} = 3$ kHz. It corresponds to the use of a pure integrator in the feedback loop. The measured frequency combs exhibit phase noise which is

TABLE III. Values of the integrated rms frequency jitter on the two defined ranges for the different lasers tested.

Laser	[0.1; 3] kHz	[3; 1000] kHz
cw NKT	0.86	0.40
cw OEWaves	0.10	0.08
Pulsed laser 1	9.23	0.65
Pulsed laser 2	0.65	0.09
Pulsed laser 3	15.98	0.35

good enough at high frequencies, even if it is limited by the measurement of floor noise. The relatively large phase noise below 20 kHz of lasers dubbed 1 and 3 are most likely mainly driven by residual coupling to environmental noise. It is observed that a 3-kHz bandwidth feedback based on a simple integrator is not sufficient to reduce the rms frequency jitter down to an acceptable level for these two lasers—in that case, $2\delta f_{\mathrm{rms}} > \Delta f$. Improved feedback schemes, as adding an additional integrator in the feedback loop, would likely be necessary to efficiently lock this laser to the POP experiment optical cavity. Laser 2, however, exhibits an excellent overall phase noise and is thus the natural candidate for its implementation in the GF POP.

The amplification scheme is based on chirped pulse amplification [46]. Two approaches are considered at this stage of the project. The first consists of a three-stage, all-fiber power amplifier, as already implemented in previous experiments [16,17]. This solution, however, requires to put the emphasis on the robust operation of such a system. It must be, in particular, fully remotely operated and failure-safe. Those are the critical aspects for their implementation in the SPS. In addition, dedicated means to tune the pulse duration, e.g., by adapting the stretching with thermally controlled fiber Bragg grating [47] could be implemented. They would allow for dynamically optimizing the laser pulse duration, as well as the laser pulse energy by controlling amplifier pump power, to achieve the maximal excitation rate of the ions by the laser photons [38]. Alternatively, an approach combining both fiber and bulk amplification stages would bring the flexibility to tune the spectral bandwidth and thus the pulse duration [48]. This kind of system can now be found as a well-proved industrial product that can operate routinely. If implemented, it could mitigate the risk related to the robustness of the laser system operation.

Finally, the amplifier must not increase the phase noise of the oscillator and have a good transverse profile so that the amplified laser beam can be efficiently coupled to the Fabry-Perot cavity longitudinal and transverse modes. Past experience shows that this is the case for both considered amplification schemes [16,49].

B. Fabry-Perot cavity design

According to the results shown in the previous paragraph, we assume that a 10,000 finesse optical resonator for operations at 40 MHz can be implemented in the SPS. Assuming that power absorption losses on the mirror coatings are maintained at a level of $A_1 = A_2 = 10^{-6}$ and diffraction losses limited to a level of $D_1 = D_2 = 10^{-5}$ per mirror, the maximum achievable enhancement on a two-mirror optical cavity is about 6000. Indeed, the finesse $\mathcal{F} \approx 2\pi/\mathcal{L}$ [50], where $\mathcal{L} = A_1 + A_2 + D_1 + D_2 + T_1 + T_2$ is the sum of all round trip losses including both mirror transmissions T_1 and T_2, thus determines the sum of mirror transmissions in intensity. The enhancement factor $G \approx 4T_1/\mathcal{L}^2$ of the optical cavity can then be adjusted by adjusting T_1 and T_2 accordingly to keep $\mathcal{F}$ and thus $\mathcal{L}$ constant. As a matter of consequence, the cavity is not necessarily impedance matched [50]. We shall assume in the following that the cavity can be designed such that it satisfies the above performance requirements, albeit with an input coupler with a transmission of $T_1 = 5 \times 10^{-4}$. In such a configuration, a 10000 finesse and a power enhancement of 5000 can be reached. The transmission of the output coupler should amount to a value of 1×10^{-4}.

The GF POP experiment needs to store up to 200 kW in the FPC which corresponds to 5-mJ pulse energy at 40 MHz. It requires a procurement of a seed laser with a power of about 60 W, assuming roughly 70% of power coupling. It is the product of two contributions. The first one is related to the so-called transverse coupling defined by the time averaged overlap, at the input mirror, of the injected laser field $\mathcal{E}_i(x, y, z_0, t)$ and that circulating in the optical cavity $\mathcal{E}_c(x, y, z_0, t)$ by

$$\left\langle \frac{|\int_{\mathcal{A}} \mathcal{E}_c(x,y,z_0,t)\mathcal{E}_i(x,y,z_0,t)dxdy|^2}{|\int_{\mathcal{A}} \mathcal{E}_c(x,y,z_0,t)dxdy|^2 |\int_{\mathcal{A}} \mathcal{E}_i(x,y,z_0,t)dxdy|^2} \right\rangle_t$$

where the symbol $\int_{\mathcal{A}}$ denotes the integral over the area $\mathcal{A}$ of the input mirror. The second one is related to the longitudinal coupling, i.e., the phase noise of the laser, estimated in the previous section. Departure larger intracavity power could be reached provided that a larger average laser power can be delivered with good quality.

The length of the FPC must be tunable so that its round-trip frequency (free spectral range) matches a frequency equal to an integer harmonic of the bunch repetition rate and the ion revolution frequency. In order to achieve this, at least one of the mirrors of the FPC must be motorized. This adjustment is usually done only once for a long period of time if the reference frequency and the FPC are stable enough. The choice of the technology for this actuator depends on how frequently tuning needs to be done, the radiation hardness of the components, and their vacuum compatibility. An annular piezoceramics equips the rear side of one of the mirrors in order to electronically lock the FPC on the reference frequency which is a harmonic of the ion revolution frequency. In order to avoid injecting noise into the piezoelectric actuator, it will operate at low voltages, typically less than 12 V. The relative tuning

range of the cavity in the synchronization loop of the FPC will thus be limited to approximately 10^{-8}. This translates directly to the necessary frequency stability of the rf reference at 40 MHz of $\Delta f_{40} \approx 0.5$ Hz.

A two-mirror geometry greatly simplifies the mechanical integration of the system compared to a four-mirror geometry and allows sufficiently precise prealignment procedures to be performed on the ground, before a careful installation in the tunnel, where either the alignment could be quickly corrected by manual operation, or remotely performed by integrating proper motorized mounts and dedicated diagnostics. Both options need to be investigated taking into account the risks of dust particle pollution of the FPC, an increase in complexity of the mechanical implementation, and potential slight vacuum degradation. The *in situ* alignment would on the contrary be necessary for a four-mirror geometry. The two-mirror geometry is well adjusted to the Gamma Factory POP experiment needs since the hadronic beam has relatively large transverse beam sizes and thus the laser beam size at the interaction point does not exhibit extreme sensitivity to the cavity length. As a consequence, the laser beam is not required to be focused down to tens of micrometers, in contrast to inverse Compton scattering experiments where laser beams are colliding with low emittance electron beams. This choice also allows for minimization of the crossing angle between the ion and laser beams, and thus improve the geometrical overlap in between laser pulses and hadronic bunches of few tens of centimeter lengths. It must be noted that similar two-mirror cavities have already been implemented in accelerator environments [51,52] allowing to reach a few degrees of crossing angle. The cavity will be implemented on a heavy, granite table to damp ground related mechanical vibrations and provide high thermal inertia. The mirror mounts will be mounted on heavy arms supported by the granite table and cantilevered at the vertical of the beam while being decoupled mechanically from the accelerator vacuum pipe to avoid transmitting related vibrations since a high mechanical stability of the system is required due to the relatively high finesse of the optical cavity. A schematic view of the optical cavity with vacuum chambers and pumps supported by the granite table is shown in Fig. 4.

C. Optical parameters at IP

Among two-mirror Fabry-Perot cavities, the hemispherical or confocal geometries could be envisaged. From a practical point of view, especially for the alignment of the system, the nearly hemispherical version seems easier to implement. Given the length of this optical cavity, driven by its synchronization to the ion beam, the only remaining parameter is the radius of curvature R of the spherical mirror in the plano-concave geometry. The $1/e^2$ transverse size of the laser beam intensity versus the position of the plane in the FPC is shown in Fig. 5. With a 10 m radius of curvature, the divergence at the geometrical center of the FPC is $< 100\ \mu$rad. The fluence on the plane mirror is below 0.15 J/cm^2 for radii of curvature above 7 m and pulse energy of 5 mJ.

D. Influence of mode degeneracy

One is interested in maximizing the overlap of the laser and ion beams, thus interested in preserving a fundamental Gaussian eigenmode in the optical cavity. However, some optical cavity transverse eigenmodes can resonate along with the fundamental Gaussian mode for a given cavity length or free spectral range [53]. These higher order modes can be seeded not only by transverse and angular misalignments but also by scattering occurring at the cavity mirrors [54] and facilitated by high average stored power that induces thermal deformations of mirror substrates. This has been observed in the past in works related to gravitational wave interferometers [55] and also in the context of high power, pulsed laser, and Fabry-Perot cavities for Compton back-scattering experiments which are closely related to the Gamma Factory concept [39]. For the two-mirror hemispherical geometry considered for the Gamma Factory POP experiment, the cylindrical symmetry being preserved, Laguerre-Gauss eigenmodes are expected to resonate. The resonance condition reads

$$2\pi p = (2n+1)\ \arccos\{\mathrm{Tr}[M(P)]/2\}, \tag{1}$$

where $\mathrm{Tr}[M(P)]$ denotes the trace of the ABCD round-trip matrix under the paraxial approximation at an average stacked power P [56,57]. Residual mirror absorption in the mirror's coatings induces thermal expansion of the substrates that can be modeled in a first approximation with the Winkler model [58]. It allows to account, in a first approximation, for the change of radius of curvature of the mirror due to absorbed power. The ABCD matrix can thus be calculated in presence of high average power in the optical cavity and the expression for the Gouy phase [59] of the Laguerre-Gauss mode of order n can be linearized in A_1P and A_2P, where $A_{1,2} \approx 10^{-6}$ is the residual power absorption of the mirror coatings and the subscript denotes the input (1) and output (2) coupler of the FPC. The high-power induced shift in Gouy phase for the fundamental mode of the Fabry-Perot cavity is naturally compensated by the feedback system. We thus look for every transverse mode of index n the smallest value of power $P = P_n$ for which the Gouy phase shift with respect to the fundamental mode $\Delta\phi_n(P) = \phi_n(P) - \phi_0(P)$

$$\Delta\phi_n(P) = 2n \arccos\left(1-\frac{2L}{R}\right) - 2nP\frac{A_2\alpha_2\kappa_1 LRw_1^2 - A_1\alpha_1\kappa_2 L^2 w_2^2 + A_1\alpha_1\kappa_2 LRw_2^2}{2\kappa_1\kappa_2\pi w_1^2 w_2^2\sqrt{L(R-L)}}, \tag{2}$$

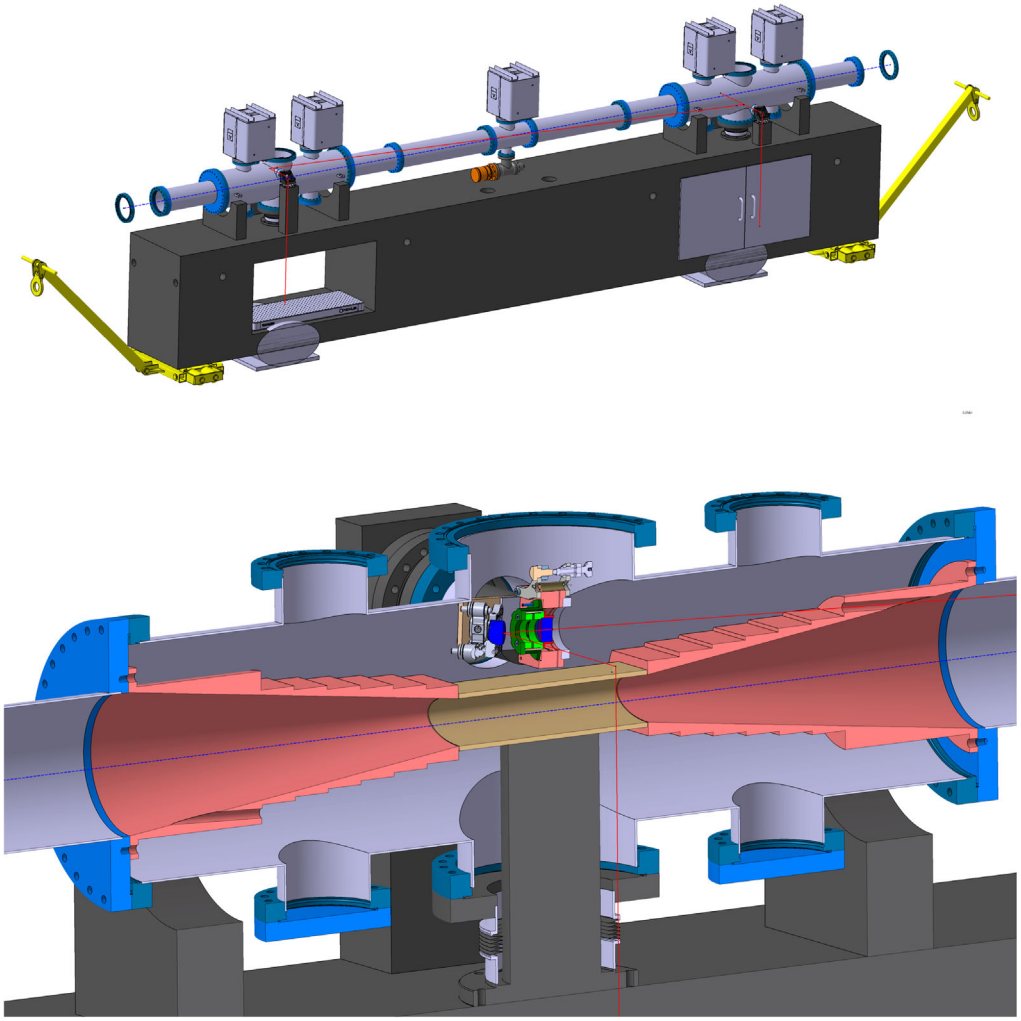

FIG. 4. Top: mechanical frame of the FPC including the vacuum chambers, the pumping system, and the granite support. The holes in the granite allow placing foreseen laser beam diagnostics within the frame itself. These holes will be closed with interlocked doors for usual operation to ensure the following laser safety regulation. The schematic shows the transport system based on air cushion systems. Bottom: inside of the vacuum chamber showing the shield of the electron beam (pink and brown) partly supported by the granite girder. The cavity and injection mirror are supported by cantilevered support mechanically decoupled from the vacuum chamber but supported by the granite frame. The thin red line represents the laser path. Mirrors outside the main vacuum chamber are not represented to ease the reading of the figure.

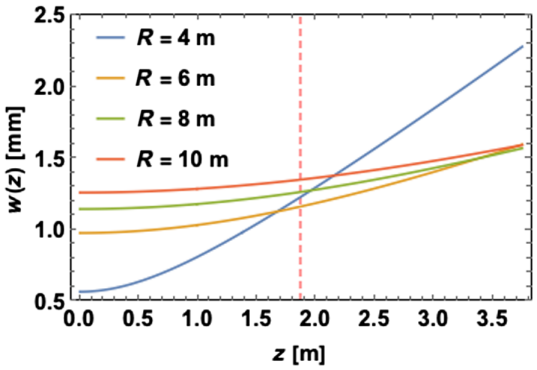

FIG. 5. The transverse size at $1/e^2$ of the intensity distribution of the laser beam inside the optical cavity. The position $z = 0 (z \simeq 3.75\text{m})$ corresponds to that of the plane (spherical) mirror. The geometrical center of the FPC is represented by the vertical dashed line.

vanishes. We denote $w_{1,2}$ the beam radii on the injection and output couplers of the FPC, $\alpha_{1,2}$ and $\kappa_{1,2}$ the thermal expansion coefficient, and thermal conductivity of their substrates, respectively. In practice, the small dilatation of the mirrors at the center induces a small reduction of the cavity length

$$\Delta L = -\left(\frac{\alpha_1 A_1}{4\pi\kappa_1} + \frac{\alpha_2 A_2}{4\pi\kappa_2}\right) P. \tag{3}$$

Anticipating that the input coupler is made of fused silica, $\alpha_1 \approx 6 \times 10^{-7}$ K^{-1} and $\kappa_1 \approx 1.38$ W/Km, and the output coupler of ultralow expansion (ULE) glass, $\alpha_2 \approx 1 \times 10^{-8}$ K^{-1} and $\kappa_2 \approx 1.31$ W/Km, one obtains $\Delta L \approx 7$ nm for $P = 200$ kW.

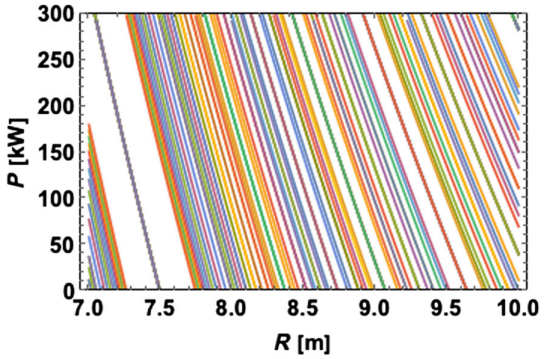

FIG. 6. The value of power at which degeneracy occurs as a function of the radius of curvature of the output coupler for mode orders from $n = 1$ to 50. Each line corresponds to a given degenerate high-order mode. The presence of degenerate high-order mode is nearly dense. Only narrow ranges of mirror radius of curvature exhibit the possibility to reach several tens of kW of average intracavity power without the occurrence of mode degeneracy.

The corresponding values of P_n are calculated as a function of the design radius of curvature of the output coupler R and shown in Fig. 6. It is found that about $P =$ 150 kW may be reached for a radius of curvature slightly larger than 7.5 m. The model employed here being approximate, the proposed optical setup needs to be assembled and experimentally validated.

Mode degeneracy is mitigated by inserting a high-order mode damper composed of D-cut mirrors that are placed at 4 mm from the beam center close to the input coupler, similarly to what was implemented in the past [39]. The cavity gain for low order modes is preserved while goes below unity for Laguerre-Gauss modes above $n = 6$. However, Hermite-Gauss modes are also possible since the cylindrical symmetry is broken by the insertion of these two HOM dampers. Hermite modes of orders $m + n > 18$ are damped with unity or less gain. The corresponding power of occurrence of the degeneracy for modes that are not damped is shown in Fig. 7, showing that the operation

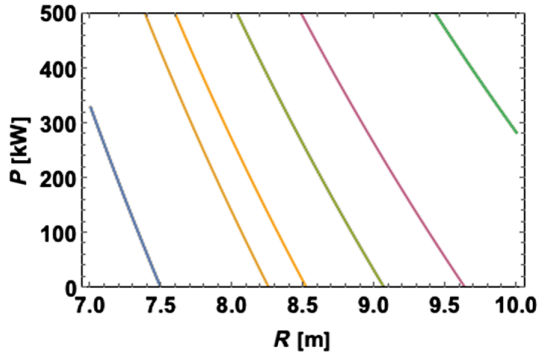

FIG. 7. The value of power at which degeneracy occurs as a function of the radius of curvature of the output coupler for mode orders from $m + n = 1$ to 18.

TABLE IV. Summary of optical cavity parameters.

Parameter name	Value
Scattering loss (in power) per mirror ($D_1 = D_2$)	$<10^{-5}$
Coating power absorption per mirror ($A_1 = A_2$)	$<10^{-6}$
Input mirror power transmission T_1	5×10^{-4}
Output mirror power transmission T_2	1×10^{-4}
Output mirror radius of curvature R	7.65 m
Laser beam waist w	1.1 mm
Average power P	>200 kW

of a 200 kW is feasible for a radius of curvature in the range of [7.5,7.8] m. A similar calculation shows that operation at this average power might be possible with a fused silica output coupler, provided that the radius of curvature is in the range of [7.5,7.6] m. However, the model developed here suffers from several approximations, which need experimental validation. We thus consider building a cavity with a radius of curvature of 7.65 m and made of ULE.

E. Summary

Following the above discussion, we summarize the specification of the optical cavity parameters in Table IV.

IV. CONCLUSION

The design of the laser system for the Gamma Factory POP experiment has been described, according to past experience. This system is based on a commercial laser oscillator amplified to 60 W and stacked in an external enhancement optical cavity with a two-mirror hemispherical geometry. Its design parameters are summarized in Table IV. We show that by mitigating effects related to mode degeneracy in the thermally load optical cavity, more than 200 kW of average power can be stored. The performance of the system remains to be demonstrated experimentally with this specific optical configuration though similar performance has been obtained in four-mirror optical cavities. Overall operational robustness must also be validated before implementation in the CERN Super Proton Synchrotron.

ACKNOWLEDGMENTS

The authors thank colleagues who more widely contribute to different and various aspects of the Gamma Factory project. The authors are thankful to Amplitude Laser Group, Light Conversion (Flint oscillator), and Menhir Photonics AG for permitting the laser phase noise measurements realized during the preparation of this paper.

[1] M. W. Krasny, The gamma factory proposal for CERN, arXiv:1511.07794.

[2] D. Budker, J. R. C. López-Urrutia, A. Derevianko, V. V. Flambaum, M. W. Krasny, A. Petrenko, S. Pustelny, A. Surzhykov, V. A. Yerokhin, and M. Zolotorev, Atomic physics studies at the gamma factory at CERN, Ann. Phys. (Berlin) **532**, 2000204 (2020).

[3] V. V. Flambaum, J. Jin, and D. Budker, Resonance photoproduction of pionic atoms at the proposed Gamma Factory, Phys. Rev. C **103**, 054603 (2021).

[4] D. Nichita, D. Balabanski, P. Constantin, W. Krasny, and W. Placzek, Radioactive ion beam production at the gamma factory, Ann. Phys. (Berlin) **534**, 2100207 (2022).

[5] D. Budker *et al.*, Expanding Nuclear Physics Horizons with the Gamma Factory, arXiv:2106.06584.

[6] V. G. Serbo, A. Surzhykov, and A. Volotka, Resonant scattering of plane-wave and twisted photons at the gamma factory, Ann. Phys. (Berlin) **534**, 2100199 (2022).

[7] M. W. Krasny, A. Petrenko, and W. Płaczek, High-luminosity Large Hadron Collider with laser-cooled isoscalar ion beams, Prog. Part. Nucl. Phys. **114**, 103792 (2020).

[8] F. Karbstein, Vacuum birefringence at the Gamma Factory, Ann. Phys. (Berlin) **534**, 2100137 (2022).

[9] B. Wojtsekhowski and D. Budker, Local lorentz invariance tests for photons and hadrons at the gamma factory, Ann. Phys. (Berlin) **534**, 2100141 (2022).

[10] S. Chakraborti, J. L. Feng, J. K. Koga, and M. Valli, Gamma factory searches for extremely weakly interacting particles, Phys. Rev. D **104**, 055023 (2021).

[11] R. Balkin, M. W. Krasny, T. Ma, B. R. Safdi, and Y. Soreq, Probing axion-like-particles at the CERN gamma factory, Ann. Phys. (Berlin) **534**, 2100222 (2022).

[12] A. Apyan, M. W. Krasny, and W. Placzek (to be published).

[13] M. W. Krasny, A. Abramov, S. E. Alden, R. Alemany Fernandez, P. S. Antsiferov, A. Apyan, H. Bartosik, E. G. Bessonov, N. Biancacci, J. Bieron *et al.* (Gamma Factory Study Group), Gamma Factory Proof-of-principle experiment, CERN, Geneva, Technical Report No. CERN-SPSC-2019-031, 2019, https://cds.cern.ch/record/2690736.

[14] L. Federici, G. Giordano, G. Matone, G. Pasquariello, P. G. Picozza, R. Caloi, L. Casano, M. P. De Pascale, M. Mattioli, E. Poldi, C. Schaerf, M. Vanni, P. Pelfer, D. Prosperi, S. Frullani, and B. Girolami, Backward Compton scattering of laser light against high-energy electrons: The LADON photon beam at Frascati, Il Nuovo Cimento B (1971-1996) **59**, 247 (1980).

[15] B. Günther, R. Gradl, C. Jud, E. Eggl, J. Huang, S. Kulpe, K. Achterhold, B. Gleich, M. Dierolf, and F. Pfeiffer, The versatile X-ray beamline of the Munich Compact Light Source: Design, instrumentation and applications, J. Synchrotron Radiat. **27**, 1395 (2020).

[16] I. Chaikovska, K. Cassou, R. Chiche, R. Cizeron, P. Cornebise, N. Delerue, D. Jehanno, F. Labaye, R. Marie, A. Martens *et al.*, High flux circularly polarized gamma beam factory: coupling a Fabry-Perot optical cavity with an electron storage ring, Sci. Rep. **6**, 36569 (2016).

[17] K. Dupraz, M. Alkadi, M. Alves, L. Amoudry, D. Auguste, J.-L. Babigeon, M. Baltazar, A. Benoit, J. Bonis, J. Bonenfant *et al.*, The ThomX ICS source, Phys. Open **5**, 100051 (2020).

[18] F. Zomer, Y. Fedala, N. Pavloff, V. Soskov, and A. Variola, Polarization induced instabilities in external four-mirror Fabry–Perot cavities, Appl. Opt. **48**, 6651 (2009).

[19] V. A. Yerokhin and A. Surzhykov, Energy levels of core-excited 1s2l2l' states in lithium-like ions: Argon to uranium, J. Phys. Chem. Ref. Data **47**, 023105 (2018).

[20] M. H. Chen, K. T. Cheng, W. R. Johnson, and J. Sapirstein, Relativistic configuration-interaction calculations for the $n = 2$ states of lithium like ions, Phys. Rev. A **52**, 266 (1995).

[21] Y. S. Kozhedub, A. V. Volotka, A. N. Artemyev, D. A. Glazov, G. Plunien, V. M. Shabaev, I. I. Tupitsyn, and T. Stöhlker, Relativistic recoil, electron-correlation, and QED effects on the 2pj-2s transition energies in Li-like ions, Phys. Rev. A **81**, 042513 (2010).

[22] J. Sapirstein and K. T. Cheng, S-matrix calculations of energy levels of the lithium isoelectronic sequence, Phys. Rev. A **83**, 012504 (2011).

[23] S. A. Blundell, Calculations of the screened self-energy and vacuum polarization in Li-like, Na-like, and Cu-like ions, Phys. Rev. A **47**, 1790 (1993).

[24] R. Büttner, B. Kraus, K. H. Schartner, F. Folkmann, P. H. Mokler, and G. Möller, EUV-spectroscopy of beam-foil excited 14.25 MeV/u Xe^{52+} + …Xe^{49+}-ions, Z. Phys. D **22**, 693 (1992).

[25] D. Feili, P. Bosselmann, K.-H. Schartner, F. Folkmann, A. E. Livingston, E. Träbert, X. Ma, and P. H. Mokler, Measurements of 2s2S1/2–2p2P1/2 transition energies in lithium like heavy ions. III. Experimental results for Sn^{47+} and Xe^{51+}, Phys. Rev. A **62**, 022501 (2000).

[26] S. Hirlaender, R. Alemany-Fernández, H. Bartosik, N. Biancacci, T. Bohl, S. C. Cave, K. Cornelis, B. Goddard, V. Kain, M. Krasny *et al.*, Lifetime and beam losses studies of partially strip ions in the SPS ($129Xe^{39+}$), in *Proceedings of 9th International Particle Accelerator Conference (IPAC-18), Vancouver, British Columbia, Canada, 2018* (JACoW Publishing, Geneva, Switzerland, 2018), pp. 4070–4072, 10.18429/JACoW-IPAC2018-THPMF015.

[27] F. Kröger, G. Weber, S. Hirlaender, R. Alemany-Fernandez, M. Krasny, T. Stöhlker, I. Tolstikhina, and V. Shevelko, Charge-state distributions of highly charged lead ions at relativistic collision energies, Ann. Phys. (Berlin) **534**, 2100245 (202).

[28] H. Bartosik, S. Albright, R. Alemany, F. Antoniou, F. Asvesta, E. Benedetto, G. Bellodi, N. Biancacci, T. Bohl, K. Cornelis *et al.*, Injectors beam performance evolution during run 2, in *Proceedings of the 9th LHC Operations Evian Workshop, Evian, 2019* (CERN, Geneva, Switzerland, 2019), pp. 51–58, https://cds.cern.ch/record/2706427/files/CERN-ACC-2019-059.pdf.

[29] G. Buchs, S. Kundermanna, E. Portuondo-Campa, and S. Lecomte, Radiation hard mode-locked laser suitable as a spaceborne frequency comb, Opt. Express **23**, 9890 (2015).

[30] Y.-S. Jang, J. Lee, S. Kim, K. Lee, S. Han, Y.-J. Kim, and S.-W. Kim, Space radiation test of saturable absorber for femtosecond laser, Opt. Lett. **39**, 2831 (2014).

[31] S. Girard, M. Vivona, A. Laurent, B. Cadier, C. Marcandella, T. Robin, E. Pinsard, A. Boukenter, and Y. Ouerdane, Radiation hardening techniques for Er/Yb doped optical fibers and amplifiers for space application, Opt. Express **20**, 8457 (2012).

[32] N. A. P. K. Kumar, K. J. Leonard, G. E. Jellison, and L. L. Snead, High-dose neutron irradiation performance of dielectric mirrors, Fusion Sci. Technol. **67**, 771 (2015).

[33] A. Rakhman, M. Hafez, S. Nanda, F. Benmokhtar, A. Camsonne, G. Cates, M. Dalton, G. Franklin, M. Friend, R. Michaels, V. Nelyubin, D. Parno, K. Paschke, B. Quinn, P. Souder, and W. Tobias, A high-finesse Fabry–Perot cavity with a frequency-doubled green laser for precision Compton polarimetry at Jefferson Lab, Nucl. Instrum. Methods Phys. Res., Sect. A **822**, 82 (2016).

[34] H. Damerau, A. Funken, R. Garoby, S. Gilardoni, B. Goddard, K. Hanke, A. Lombardi, D. Manglunki, M. Meddahi, B. Mikulec, G. Rumolo, E. Shaposhnikova, M. Vretenar, and J. Coupard, LHC injectors upgrade, Technical Design Report, CERN, Technical Report No. CERN-ACC-2014-0337, 2014, https://cds.cern.ch/record/1976692?ln=fr.

[35] M. Schaumann *et al.*, First partially stripped ions in the LHC ($208Pb^{81+}$), in *Proceedings of the 10th International Particle Accelerator Conference (IPAC'19), Melbourne, Australia, 2019* (JACoW Publishing, Geneva, Switzerland, 2019), pp. 689–692, https://cds.cern.ch/record/2672790.

[36] F. M. Kröger, G. Weber, V. P. Shevelko, S. Hirlaender, M. W. Krasny, and T. Stöhlker, Charge state tailoring of relativistic heavy ion beams for the Gamma Factory project at CERN, X-Ray Spectrom. **49**, 25 (2020).

[37] E. Bravin, S. Burger, G. Ferioli, G. J. Focker, A. Guerrero, and R. MacCaferri, A new TV beam observation system for CERN, Technical Report No. CERN-AB-2005-076, 2005, https://cds.cern.ch/record/895159/files/ab-2005-076.pdf.

[38] J. Bieroń, M. W. Krasny, W. Płaczek, and S. Pustelny, Optical excitation of ultra-relativistic partially stripped ions, Ann. Phys. (Berlin) **534**, 2100250 (2022).

[39] L. Amoudry, H. Wang, K. Cassou, R. Chiche, K. Dupraz, A. Martens, D. Nutarelli, V. Soskov, and F. Zomer, Modal instability suppression in a high-average-power and high-finesse Fabry–Perot cavity, Appl. Opt. **59**, 116 (2020).

[40] C. Dixneuf, G. Guiraud, Y.-V. Bardin, Q. Rosa, M. Goeppner, A. Hilico, C. Pierre, J. Boullet, N. Traynor, and G. Santarelli, Ultra-low intensity noise, all fiber 365 W linearly polarized single frequency laser at 1064 nm, Opt. Express **28**, 10960 (2020).

[41] M. Kellert, U. Demirbas, J. Thesinga, S. Reuter, M. Pergament, and F. X. Kärtner, High power (< 500 W) cryogenically cooled Yb:YLF cw-oscillator operating at 995 nm and 1019 nm using E//c axis for lasing, Opt. Express **29**, 11674 (2021).

[42] R. W. P. Drever, J. L. Hall, F. V. Kowalski, J. Hough, G. M. Ford, A. J. Munley, and H. Ward, Laser phase and frequency stabilization using an optical resonator, Appl. Phys. B **31**, 97 (1983).

[43] E. Black, An introduction to Pound–Drever–Hall laser frequency stabilization, Am. J. Phys. **69**, 79 (2001).

[44] R. Jason Jones, J.-C. Diels, J. Jasapara, and W. Rudolph, Stabilization of the frequency, phase, and repetition rate of an ultra-short pulse train to a Fabry–Perot reference cavity, Opt. Commun. **175**, 409 (2000).

[45] H. Damerau *et al.*, RF synchronization and distribution for AWAKE at CERN, in *Proceedings of the 7th International Particle Accelerator Conference, IPAC-2016, Busan, Korea, 2016* (JACoW, Geneva, Switzerland, 2016), pp. 3743–3746.

[46] D. Strickland and G. Mourou, Compression of amplified chirped optical pulses, Opt. Commun. **56**, 219 (1985).

[47] X. Zhang, Z. Yang, Q. Li, F. Li, X. Yang, Y. Wang, and W. Zhao, Pulse duration tunable fiber CPA system based on thermally dispersion tuning of chirped fiber bragg grating, Optik **127**, 8728 (2016).

[48] J. Pouysegur, F. Guichard, Y. Zaouter, M. Hanna, F. Druon, C. Hönninger, E. Mottay, and P. Georges, Hybrid high-energy high-power pulsewidth-tunable picosecond source, Opt. Lett. **40**, 5184 (2015).

[49] F. Blanc, M. Amer, G. Bonamis, K. Cassou, R. Chiche, A. Courjaud, K. Dupraz, A. Martens, D. Nutarelli, Y. Peinaud, and F. Zomer, Compact kW-class enhancement cavity operated at GHz repetition rates for Inverse Compton Scattering sources, in *Proceedings of Optica High-brightness Sources and Light-driven Interactions Congress, Budapest, Hungary, 2022* (Optica Publishing Group, 2022), p. EF4A.3, https://opg.optica.org/abstract.cfm?uri=EUVXRAY-2022-EF4A.3.

[50] F. Bondu and O. Debieu, Accurate measurement method of Fabry–Perot cavity parameters via optical transfer function, Appl. Opt. **46**, 2611 (2007).

[51] T. Allison, M. Anderson, D. Androić, D. Armstrong, A. Asaturyan, T. Averett, R. Averill, J. Balewski, J. Beaufait, R. Beminiwattha *et al.*, The Qweak experimental apparatus, Nucl. Instrum. Methods Phys. Res., Sect. A **781**, 105 (2015).

[52] S. Baudrand *et al.*, A high precision Fabry–Perot cavity polarimeter at HERA, J. Instrum. **5**, P06005 (2010).

[53] D. Herriott, H. Kogelnik, and R. Kompfner, Off-axis paths in spherical mirror interferometers, Appl. Opt. **3**, 523 (1964).

[54] T. Klaassen, J. de Jong, M. van Exter, and J. P. Woerdman, Transverse mode coupling in an optical resonator, Opt. Lett. **30**, 1959 (2005).

[55] A. L. Bullington, B. T. Lantz, M. M. Fejer, and R. L. Byer, Modal frequency degeneracy in thermally loaded optical resonators, Appl. Opt. **47**, 2840 (2008).

[56] H. Kogelnik and T. Li, Laser beams and resonators, Appl. Opt. **5**, 1550 (1966).

[57] S. Gigan, L. Lopez, N. Treps, A. Maître, and C. Fabre, Image transmission through a stable paraxial cavity, Phys. Rev. A **72**, 023804 (2005).

[58] W. Winkler, K. Danzmann, A. Rüdiger, and R. Schilling, Heating by optical absorption and the performance of interferometric gravitational-wave detectors, Phys. Rev. A **44**, 7022 (1991).

[59] S. Feng and H. G. Winful, Physical origin of the Gouy phase shift, Opt. Lett. **26**, 485 (2001).